HHS Public Access

Author manuscript

Small. Author manuscript; available in PMC 2020 January 12.

Published in final edited form as:

Small. 2018 May ; 14(18): e1702945. doi:10.1002/smll.201702945.

Characterization of Membrane Patch (MP) - Ion Channel Probes (ICPs) for Scanning Ion Conductance Microscopy

Wenqing Shi[1,†], **Yuhan Zeng**[1,†], **Cheng Zhu**[1], **Yucheng Xiao**[2], **Theodore R. Cummins**[2], **Jianghui Hou**[3], **Lane A. Baker**[*,1]

[1]Department of Chemistry, Indiana University, 800 E. Kirkwood Avenue, Bloomington, Indiana 47405

[2]Department of Biology, Indiana University-Purdue University Indianapolis, Stark Neurosciences Research Institute, 723 West Michigan Street, SL-306 Indianapolis, Indiana 46202

[3]Department of Internal Medicine – Renal Division, Division of Biological and Biochemical Sciences, Washington University School of Medicine, 660 South Euclid Avenue, Campus Box 8126, St. Louis, Missouri 63110

Abstract

Integration of dual-barrel membrane patch-ion channel probes (MP-ICPs) to scanning ion conductance microscopy (SICM) holds promise of providing a revolutionized approach of spatially-resolved chemical sensing. However, to fully exploit the MP-ICP platforms for concurrent topography and chemical sensing, a comprehensive characterization of the analytical performance of this newly-developed platform is needed.

In this report, a series of experiments were performed to further our understanding of the system and to answer some fundamental questions, in preparation for future developments of this approach. First, we constructed MP-ICPs that contained different types of ion channels including TRPV1 and BK channels to establish the generalizability of the methods. Next, we proved the capability of the MP-ICP platforms in single ion channel activity measurements, and demonstrated that the channel behaviors can be faithfully obtained with this approach. In addition, we studied the interplay between the SICM barrel and the ICP barrel. For ion channels gated by uncharged ligands, channel activity at the ICP barrel is unaffected by the SICM barrel potential; whereas for ion channels that are gated by charged ligands, enhanced channel activity can be obtained by biasing the SICM barrel at potentials with opposite polarity to the charge of the ligand molecules. Finally, a proof-of-principle experiment was performed and site-specific molecular/ionic flux sensing was demonstrated at single-ion-channel level, which showed that the MP-ICP platform can be used to quantify local molecular/ionic concentrations.

INTRODUCTION

Investigation of dynamic chemical events such as specific ion efflux/influx through ion channels or exocytosis of neurotransmitters at cellular surfaces has attracted broad interest,

[*]Author to whom correspondence should be addressed., [1] lanbaker@indiana.edu; Phone: (812) 856-1873; Fax: (812) 856-8300.
[†]These authors contributed equally to this work.

as knowledge of such dynamic events is key to reveal mechanistic details of many biological processes. Electrochemical approaches such as amperometry and fast scan cyclic voltammetry have been widely-employed to measure exocytotic release of electroactive species at single-cell level. In the pioneering work of Wightman and co-workers, detection of stimulated secretion of catecholamines from chromaffin cells has been obtained *via* carbon fiber microelectrodes (CFMEs) positioned at micrometer distances from the cell of interest. In such amperometric recordings, the potential applied to the CFME was biased at a sufficient value to oxidize catecholamine at the CFME surface, resulting in a series of current spikes with each peak representing a single exocytotic event.[1, 2] In subsequent studies, electrochemical detection methods *via* CFMEs have been widely-used for real-time measurements of cellular releasates including dopamine, serotonin, histidine, insulin, and others, providing important insights into exocytosis processes.[3–8]

Powerful as such cellular measurement are, two major caveats exist for this approach. First, a typical CFME has a diameter of 5 μm, which is of similar size to the cells being measured, rendering sub-cellular spatial resolution difficult to obtain. Second, the secretory analytes must be electroactive to be detected, and, thus, only a limited number of transmitters are amenable to analysis.

Alternatively, detection of acetylcholine (ACh) secretion from growth cones of single neurons has been demonstrated with the so-called “sniffer-patch” technique.[9–11] In brief, an isolated patch of receptor-rich (i.e., acetylcholine receptor, AChR) membrane was excised from a donor cell in an outside-out patch configuration.[12] Receptors within the membrane were used to measure the neurotransmitter release. In comparison to CFMEs, the use of ion channel receptors as specific molecular sensors directly exploits the high affinity of ligand-gated ion channels to their native neurotransmitters, expanding the detection regime to molecules with little to no electrochemical activity.

However, the precision of manual probe control in the measurements with CFMEs or “sniffer-patch” is unfavorable for high spatial resolution measurements. Ideally, the sensor position needs to be controlled with nanometer-precision in x, y and z dimensions. In x–y dimension, positional accuracy is vital to pinpoint discrete loci within the cell membrane to obtain site-specific signals. In z dimension, the sensor should be positioned in proximity to the site of release, as the concentration of the released molecules decreases sharply with distance due to the diffusion smearing effects.[11, 13]

Numerous attempts have been undertaken to provide a spatially resolved view of chemical events. For instance, integration of microelectrodes (i.e., carbon, Pt, Au) with scanning electrochemical microscopy (SECM) has enabled concurrent topography and electrochemical activity imaging in biological systems, albeit the detection range is still only limited to electroactive analytes. Work here takes cues from nanopore platforms (i.e., biological nanopores or solid-state nanopores) that have been widely employed for various sensing applications.[14] In an alternative route described by Zhou et al., ion channel probes (ICPs), in which micropipettes modified with an artificial lipid bilayer that contained multiple ion channels (i.e., alpha hemolysin, α-HL) have been integrated with SICM, and preliminary results demonstrated the utilization of ICPs for topographical imaging.[15] In a

following work, concurrent imaging and sensing of cyclodextrin with a similar micron-sized probe was reported.[16] However, the major limitation in the aforementioned reports is that the signal used for feedback and chemical sensing both came from the ion current through the ion channels, and, thus, the feedback imaging and the chemical sensing were largely coupled. As a result, the ion current either served solely as feedback for topographical imaging as in Zhou et al.;[15] or only be used for chemical sensing as in Macazo et al., where the topography was collected in constant-height mode without any feedback.[16]

To decouple the current for feedback imaging and ion channel sensing, a new platform, dual-barrel membrane patch-ion channel probes (MP-ICPs), comprised of two barrels, with an open barrel used for SICM imaging and a barrel with a membrane patch containing ion channels of interest for chemical sensing, has been developed. The open barrel (SICM barrel) serves to measure the distance-dependent ion current for probe positioning and non-invasive imaging *via* the same feedback mechanism as in traditional SICM.[17, 18] The second barrel in the probe supports the membrane patch (ICP barrel) and is used to study ion channel activities. In our initial report, the mechanical and electrical stability of the membrane patches, as well as the individual addressability of the two barrels have been proven. Moreover, ion channel activity of a ligand-gated ion channel with respect to the vertical distance between the channel and the ligand source was measured, and distinct characteristics were observed when the probe was close to and far from the ligand source, further highlighting the importance of robust probe position control in the studies of ion channel activities.[19]

In theory, MP-ICPs can be employed to spatially map any signaling molecules provided if a suitable ion channel can be found to be used as a sensor, which can significantly diversify the biochemical systems and targets to be investigated. Additionally, this innovative platform may offer orders-of-magnitude increases in the sensitivity, spatial, and temporal responses of the measurements, and, thus, the analytical performance of this platform should be carefully accessed.

To do so, we performed a series of experiments, detailed herein. First, to demonstrate the generic nature of the MP-ICP platforms, probes with the ICP barrel containing excised patches with different types of ion channels such as BK (large conductance Ca^{2+}-activated K^{+}) channels[20] or TRPV1 (transient receptor potential vanilloid 1) channels[21] were prepared. Amperometric current-time (I–T) recordings were performed to monitor the channel activities at the ICP barrel, and ion current modulations resulting from the open/close of single or multiple ion channels were clearly observed, which validated the single channel recording capability of the system. Moreover, to fully understand the interplay between the SICM barrel and the ICP barrel, the open probability (P_{open}) of the ion channels within the ICP barrel was measured as a function of the potential applied to the SICM barrel. The charge of the ligand molecules was found to be central to whether or not the potential at the SICM barrel will influence the ICP barrel channel activities. Furthermore, a proof-of-principle experiment was performed to demonstrate the feasibility of measuring site-specific molecular/ionic flux (i.e., capsaicin or Ca^{2+}) with single ion channels (i.e., TRPV1 channel or BK channel).

EXPERIMENTAL

Chemicals and Materials

Sodium chloride (VWR, Radnor, PA); potassium chloride (Macron Chemicals, Phillipsburg, NJ); magnesium chloride hexahydrate (J. T. Baker, Phillipsburg, NJ); calcium chloride dihydrate (Sigma-Aldrich, St. Louis, MO); ethylenediaminetetraacetic acid (EDTA) (Sigma-Aldrich); ethylene glycol-bis(2-aminoethylether)-N, N, N′, N′-tetraacetic acid (EGTA) (Sigma-Aldrich) and 4-(2-hydroxyethyl)-1-piperazineethanesulfonic acid) (HEPES) (Sigma-Aldrich) were used to prepare the electrolyte solutions. Capsaicin (purity > 95%, Cayman Chemical, Ann Arbor, MI) was dissolved in ethanol and stored at −20°C prior to use. On the day of experiment, the ethanol solvent was removed and the capsaicin was dissolved in aqueous recording buffers, and used for TRPV1 channel excitations. All chemicals were used as received without further purification. Hydrochloric acid (EMD Millipore, Billerica, MA) and aqueous solutions of potassium hydroxide (Mallinckrodt, St. Louis, MO) and sodium hydroxide (EMD Millipore) were used for buffer pH adjustment. All aqueous solutions were prepared with deionized water (resistivity = 18 MΩ · cm at 25°C, EMD Millipore) and were filtered with 0.22 μm PVDF filter membranes (EMD Millipore) prior to use.

Cell Culture and Transfection

Human embryonic kidney 293 (HEK 293) cells were grown under standard tissue culture conditions (5% CO_2 and 37°C) in Dulbecco's Modified Eagle's Medium (DMEM-high glucose, D6429, Sigma-Aldrich, St. Louis, MO) supplemented with 10% (v/v) fetal bovine serum (F4135, Sigma-Aldrich) and 1% penicillin-streptomycin (P0781, Sigma-Aldrich).

Preparation of Transient Transfected Cell Lines—The cDNAs encoding human BK channel or TPRV1 channel were subcloned into pcDNA3.1 vector. The cDNA encoding GFP protein was subcloned into pEGFP vector. Transfection grade vectors were purified from *Escherichia coli*. The BK or TRPV1 vector was co-transfected with the GFP vector into HEK293 cells with the calcium phosphate precipitation method.[22] The transfected cells were cultured for 48 h to allow transgene expression and GFP visualization. In the experiments, fluorescent cells were selected for patch-clamp measurements, where co-expression of GFP was used as a marker of successful transfection of ion channels of interest. In Figure 1a, an overlaid fluorescent and bright-field image of HEK 293 cells transfected with GFP and TRPV1 channel is shown. The corresponding bright-field image after formation of tight seal between the probe and the target cell is shown in Figure 1b, a red arrow was added in Figure 1b to indicate the position of the dual-barrel probe for better visualization.

Preparation of Stably Transfected Cell Lines—Wild type GFP-tagged human potassium large conductance calcium-activated channel (KCNMA1, OriGene) was transfected into HEK293 cells by the calcium phosphate precipitation method as described previously (Xiao et al., 2008). After transfection for 5 h, the cells were washed with fresh medium. After 48 h, antibiotic (G418, Geneticin; Cellgro, Herndon, VA) was added to select for neomycin-resistant cells. After 2–3 weeks in G418, colonies were picked, split, and

subsequently tested for channel expression using whole-cell patch clamp recording techniques.[23]

Instrumentation and Probe Construction

In Figure 1c, a scanning electron micrograph of a typical dual-barrel probe used in the experiments is shown. We have found electrodes that are submicron in pore opening, but hundreds of nanometers in dimension provide a good balance between patch formation, probability of trapping single channels, and probe feedback/control in SICM. The fabrication and characterization procedure of the dual-barrel pipettes used in our experiments has been detailed in a previous report.[19] To realize MP-ICP-SICM, the dual-barrel probe was mounted vertically on a piezoelectric positioner of a scanIC scanning ion conductance microscope (Ionscope Ltd., London, UK) and manipulated *via* the SICM software. Figure 1d depicts the schematic illustration of the instrument setup of the MP-ICP-SICM. Each barrel of the dual-barrel probe contained an individually-addressable Ag/AgCl electrode, namely, **WE1** and **WE2**, and the two electrodes shared a common reference electrode (**RE**, Ag/AgCl) in the bath solution, which was held at ground. One of the two barrels of the theta pipette (with **WE1** back-inserted) was connected to the headstage of an Axopatch 200 current amplifier (Molecular Devices, Sunnyvale, CA), termed as SICM barrel. A second current amplifier (PC505B, Warner Instrument, Hamden, CT) was employed to apply potential and monitor current of the second barrel (with **WE2** back-inserted), hereafter defined as ICP barrel.

The construction steps of a MP-ICP probe have been detailed in our previous work.[19] In brief, after the formation of gigaseal (i.e., tight seal between cell membrane and the glass wall) on both barrels, retraction of the probe away from the patched cell led to the formation of inside-out patches on both barrels.[12] Next, electrically-induced breakdown was performed *via* the application of pulse potentials to **WE1** to break the membrane patch at the SICM barrel. The two barrels are individually-addressable, and, as a result, the membrane patch on the ICP barrel remained intact. In the final probe configuration, current flow between the **WE1** in the open barrel and **RE** in the bath solution was used as feedback to control the probe-substrate distance; and the ICP barrel contained a membrane patch with ion channels of interest to sense specific chemicals through amperometric measurements. Currents were low-pass filtered at 1 kHz (−3 dB, 4-pole Bessel) and sampled at either 4 kHz (SICM barrel) or 50 kHz (ICP barrel). Data were acquired with Digidata 1440A (SICM barrel) and Digidata 1550 4B (ICP barrel) digitizers (Molecular Devices).

Ion Channel Recordings

Inside-out patch recordings from HEK 293 cells constructed with TRPV1 channels were performed in equimolar Na^+ buffer in both the pipette and the bath. The pipette solution consisted of 140 mM NaCl, 2 mM $MgCl_2$, 1.1 mM EGTA and 10 mM HEPES (pH was adjusted to 7.2 with NaOH). For each experiment, the bath solution was freshly prepared by addition of capsaicin in the Na^+ buffer, and used the day of experiment.

Inside-out patch recordings from HEK 293 cells constructed with BK channels were performed when the pipette was filled with solution consisted of 140 mM KCl, 5 mM NaCl,

10 mM HEPES and 1.1 mM EGTA (buffered at pH = 7.2 with KOH). In the bath solution, 140 mM KCl, 5 mM NaCl, 2 mM $MgCl_2$, 1 mM $CaCl_2$ and 10 mM HEPES were used an the solution was buffered at pH = 7.4 with KOH.

In the experiments to investigate the influence of the SICM barrel potential on the channel activities at the ICP barrel, the bias applied to the SICM barrel was held at −10 mV, −5 mV, 0 mV, +5 mV and +10 mV. Meanwhile, I–T measurements were performed at the ICP barrel when the bias was kept constant, and the resultant I–T traces were used for further statistical analysis to reveal channel activities (i.e., open probability).

To measure site-specific capsaicin or Ca^{2+} flux, a nanopore or micropore within a polyimide (PI) membrane separating two electrolyte-filled reservoirs was used as a capsaicin or Ca^{2+} source. The top reservoir was filled with extracellular buffer, whereas the bottom reservoir contained extracellular buffer together with capsaicin (for TRPV1 channels) or Ca^{2+} (for BK channels), such that capsaicin molecules or Ca^{2+} ions diffuse from the bottom reservoir to the top reservoir through the nanopore under concentration gradient. First, a topography image was obtained *via* the SICM barrel. Next, using the previous-obtained topography image as a reference, the probe was navigated and positioned at different vertical or lateral locations relative to the pore. Finally, at each locations, I–T measurements were performed and used for statistical analysis.

RESULTS AND DISCUSSION

Single Ion Channel Recordings

In our previous study, the electrical noise in the system when both the ICP barrel and the SICM barrel were connected to their corresponding current amplifiers was measured to be ~10 pA, whereas the typical baseline noise level required for single channel recordings is ~2 pA. As required, digital noise cancellation was performed with the HumSilencer adaptive noise cancellation function in the 1550 4B digitizer.

The pain receptor channel TRPV1 (i.e., the heat and capsaicin receptor) is primarily expressed by primary afferent sensory neurons of the pain pathway, and plays an important role in the detection of a wide variety of noxious stimuli, including heat (>42 °C) and various noxious chemicals, such as eicosanoids, capsaicin (the active component of chili peppers), protons and peptide toxins.[24–33] The functional channel of TRPV1 consists of four identical subunits that symmetrically arrange to form a central ion-conducting pore, as proven in cryo-EM structures.[34] To elicit channel activation, capsaicin molecules bind to vanilloid binding sites at the intracellular side of the cell membrane.[31] The Ca^{2+}-activated BK channels, comprised of four pore-forming subunits encoded by a single *Slo1* gene,[35, 36] can be activated by membrane depolarization or intracellular Ca^{2+}.[20, 37] Thus, in the experiments here, ion channel recordings were all performed in inside-out patch configurations and 1 μM capsaicin (for TRPV1 channels) and 1 or 50 mM Ca^{2+} (for BK channels) agonists were added in the bath solution. Of note, Ca^{2+} was excluded from the extracellular solution for TRPV1 channel experiments to prevent desensitization of TRPV1 channels.[21]

In these experiments, potential applied to the SICM barrel was held at 0 mV after probe position was fixed for simplification. Figure 2 shows the representative I–T traces (left) and corresponding statistical graphs (right) of current amplitude vs. dwell time (I_{open}-t_{open}) recorded *via* a single TRPV1 channel at the ICP barrel. In the I_{open}-t_{open} graphs, C represents the closed state, and O represents the open state. The membrane potential (V_m) was varied within the range of −100 mV to +100 mV. Two important factors for channel characterization were studied, namely, the current amplitude (I_{open}) and the channel open probability (P_{open}). Both I_{open} and P_{open} decreased at hyperpolarization potentials. In terms of the I_{open}, at positive V_m, i.e., +40 mV to +100 mV, I_{open} increased with increasing V_m. At +40 mV, the average open channel current was measured to be ~3.22 pA; while at +100 mV, a current of ~9.81 pA was obtained. At negative V_m, i.e., −100 mV to −40 mV, I_{open} was observed to be smaller, and current increments were more gradual as compared to those at positive membrane potentials, with ~2.87 pA at V_m = −100 mV and ~1.68 pA at V_m = −40 mV.

For TRPV channels, channel structure and gating mechanism lead to a well-known rectified current-voltage response, while for BK channels a linear response is obtained, a feature that can be used to further characterize the membrane patch,[20, 38] In Figure 3, the current-voltage (I–V) relationship derived from single TRPV1 channel recording data is shown, and a prominent outward rectification behavior was observed. From the slope of the positive half and the negative half of the I–V curve, conductances of ~90 pS at positive membrane potentials and ~30 pS at negative membrane potentials were calculated. The single channel properties obtained from our measurements agree well with those reported in previous literature,[21, 30–32] demonstrating the MP-ICPs' capability in single ion channel recordings under these conditions.

In addition, to demonstrate that the MP-ICP approach can be adapted for detection of different analytes, we also performed single ion channel recording experiments with BK channels. Figure 3b shows the I–V relationship obtained from the I–T traces, a unitary conductance of ~190 pS was obtained for transient-transfected BK channels. The I–V relationship of a stably transfected BK channel is shown in Figure S1 (Supporting Information), showing a unitary conductance of 206 pS, which is, again, in good agreement with previous literature.[39–41] For I–V relationship shown here in Figure 3, at least three measurements were repeated with good reproducibility.

Taken in total, results demonstrate the possibility of performing sensing experiments *via* a single ion channel in our system, and highlight the versatility of MP-ICP platforms.

Influence of the SICM Barrel Potential on Ion Channel Activities

The next question that we want to address is: whether there will be any interference between the two barrels ? Specifically, will the electrical field generated by the SICM barrel influence the ion channel activities observed at the ICP barrel? And if so, how will the channel activities be altered?

To understand the relationship between the two barrels, we held the ICP barrel potential constant, and measured ion channel activities at the ICP barrel as a function of the SICM

barrel potential. Both TRPV1 channels and BK channels were used for these experiments. TRPV1 channels, which are activated by capsaicin, represent neutral ligand-gated channels, as capsaicin is uncharged at physiological pH. On the other hand, BK channels, which are triggered by Ca^{2+}, represent positively-charged ligand-gated channels.

In Figure 4, statistical graphs of I_{open}-t_{open} for TRPV1 channels (left) and BK channels (right), when the SICM barrel potential was varied from −10 mV to +10 mV with 5 mV increment, are shown. The ICP barrel potential was kept at V_m = +60 mV. For TRPV1 channels, two well-defined populations, *viz.*, open state and closed state, were observed. The open state has an I_{open} amplitude of ~5.3 pA, corresponding to a unitary conductance of ~87 pS; while in the closed state, the current was presumably 0. When the SICM barrel potential was ramped from −10 mV to +10 mV, no obvious difference was observed for the distribution of the two populations, that is to say, the channel activities remained unaffected by the SICM barrel potentials. Our working hypothesis for the inertness of TRPV1 channel activities to SICM barrel potential is the uncharged nature of capsaicin molecules. First, when there is no potential applied to the SICM barrel, capsaicin molecules stochastically move towards and then activate the TRPV1 channels at the ICP barrel. Next, when a potential is applied to the SICM barrel, an electric field will be produced at the SICM barrel, which may pose either attractive or repulsive forces to the analyte molecules in proximity to the tip, and, thus, impact local analyte concentrations at the ICP barrel. However, the movement of capsaicin molecules near the tip will remain unaltered regardless of the electric field at the SICM barrel, as capsaicin molecules are uncharged, and, thus, has zero electrophoretic mobility.

To further investigate if the charge of the ligand molecule is the key factor to determine the impact of SICM barrel potential on ICP barrel's channel activities, we repeated the aforementioned experiments, using a different type of ion channel, the BK channel, which is triggered by positively-charged Ca^{2+} ions. Similar to the results for TRPV1 channels, a distinct two-state distribution was observed from the I_{open}-t_{open} graphs for BK channels. At open state, an I_{open} of ~11.1 pA was observed, which was corresponding to a unitary conductance of ~190 pS; and at closed state, the current fluctuated around zero. However, unlike the case of TRPV1 channel to different SICM barrel potentials, distinct features were observed from the two-state distributions for BK channels at different SICM barrel potentials. By comparing the two-state distributions at +10 mV and −10 mV, the open state peak became more prominent at −10 mV, meaning the channel spent more time in the open state as opposed to the closed state.

To better compare the behaviors of the two channels, P_{open} of TRPV1 channels (blue) and BK channels (red) was plotted as a function of SICM barrel potential, as shown in Figure 5. For TRPV1 channel, P_{open} remained the same at ~90%, despite the variations in SICM barrel potentials. Whereas for BK channels, when SICM barrel was biased at +10 mV, a P_{open} of ~75% was observed, at −10 mV, on the other hand, we observed a P_{open} of ~95%. The overall trend for BK channel is, as the applied potential at the SICM barrel becomes more negative, the channels become more active at the ICP barrel.

Results here demonstrate charge of ligand molecules is central to whether or not the potential at the SICM barrel will influence the channel activities at the ICP barrel. For TRPV1 channels, P_{open} remained stable at varying SICM barrel potentials. For BK channels, higher P_{open} was observed at more negative applied potentials, whereas P_{open} decreased when the applied potential was positive.

Distance-dependent Ion Channel Activities

Finally, to demonstrate the feasibility of using this approach to measure local molecular or ionic flux, a proof-of-concept experiment was performed, and the response of a single TRPV1 (or BK) ion channel at the ICP barrel was examined as a function of distance between the probe and a diffusional source of capsaicin molecules (or Ca^{2+} ions).

In the first experiment, a nanopore with a nominal diameter of ~700 nm within a synthetic membrane mounted in a diffusion cell was used as a capsaicin source, where capsaicin molecules diffuse from the bottom chamber to the top chamber under a concentration gradient (i.e., in the bottom chamber, capsaicin and the Na^+ recording buffer were present; while in the top chamber contained only the Na^+ recording buffer). SICM barrel potential was held at 0 mV. ICP barrel was held at V_m = +60 mV for ion channel recordings to measure the flux of capsaicin. Figure 6 shows the representative I–T traces and the corresponding I_{open}-t_{open} statistical graphs, when the probe was directly held over a nanopore (with zero lateral displacement relative to the pore) and laterally moved away from the nanopore by −5, −2, +2 and +5 μm. A red dashed line was added to the left of the I–T traces to indicate the closed state (C). The vertical distance between the probe and the nanopore was identical for all the measurements, i.e., ~200 nm. In Figure 6, the current amplitude at open state (O) remained the same regardless of the probe position relative to the capsaicin source. However, the open probability was strongly dependent on the relative distance between the probe and the pore. Specifically, the TRPV1 channel remained mostly in open state when the probe was directly positioned above the nanopore, viz., the 0 position. As the probe was laterally moved away from the pore, the channel activities decreased, as indicated by the decreased amount of channel opening events.

To provide a more direct view of the dependence of channel activity on the distance between the ligand source and the probe, we plotted the P_{open} as a function of the lateral distance between the probe and the nanopore, as shown in Figure 7. Relative position of the probe with respect to the pore is illustrated in the cartoon schematic. The highest P_{open}, ~95%, was observed when the probe was right above the nanopore. When the probe was ± 2 μm away from the pore, a P_{open} of ~25% was measured. As the probe was moved farther from the pore, ± 5 μm, P_{open} decreased to ~15%. The decreased P_{open} was reasoned to the decreased agonist concentration experienced by the ion channels when the probe was farther away from the agonist source.

The aforementioned results demonstrated the ability of the MP-ICP platform to measure local molecular flux with precise distance control provided by SICM. Next, local ionic diffusional flux was also analyzed with the ICP-SICM system, with BK channels. A similar setup to that shown in Figure 7 was employed. The membrane patch on the ICP barrel contained a single BK channel, and the pore in the PI membrane had a diameter of 1.9 μm.

The top and bottom chambers both contained the K^+ recording buffer for BK channel, while 50 mM Ca^{2+} was added to the bottom chamber. Ion current in the SICM barrel was used as feedback for probe-substrate distance control, and once the probe was moved to a desired position, the feedback was switched off to fix the distance, and the potential on the SICM barrel was held at 0 mV. ICP barrel was held at V_m = +60 mV for ion channel recordings to measure the diffusional flux of Ca^{2+}. The probe was approached to the PI membrane surface after the following fixed-position measurements, and the current response of the SICM barrel was recorded as a function of probe-sample distance (see Figure S2, Supporting Information). The probe-sample distances during fixed-position measurements were determined from the approach curve. The probe was first held above the pore center at different vertical distances (0.33, 0.72, 1.44, 2.15, 2.96 and 3.39 μm). Then the probe was held at a constant vertical distance (171 nm) to the pore center, while moved laterally to different positions (0, 1.56, 3.13, 4.69 and 6.25 μm) relative to the pore center.

At each fixed position, 10–30 seconds of channel activities on the ICP barrel were recorded, and the representative I–T traces and the corresponding I_{open}-t_{open} statistical graphs are shown in Figure 8a (vertical distance dependent) and Figure 9a (lateral distance dependent). In Figure 8b, the open probability P_{open} of BK channel was plotted as a function of the vertical distance between the probe and the pore center (red curve). When probe was held at a closer vertical distance (0.33 μm) to the pore center, P_{open} was ~50%, and as probe was retracted to higher distances, 0.72, 1.44, 2.15, 2.96 and 3.39 μm, P_{open} decreased to ~39%, ~25%, ~21%, ~7% and ~0.4%, respectively. In Figure 9b, P_{open} was plotted as a function of the lateral distance from probe to pore center (red curve). When probe was held right above pore center at a fixed vertical distance of 171 nm, P_{open} was ~84%, and as probe was laterally moved by 1.56, 3.13, 4.69 and 6.25 μm from pore center, P_{open} decreased to ~19%, ~17%, ~9% and ~0.4% respectively.

As proved by previous studies, P_{open} of BK channel at a fixed membrane potential increases with higher intracellular [Ca^{2+}],[41, 42] and thus different [Ca^{2+}] due to ionic diffusion from the pore gives rise to variations in P_{open} at different vertical distances. Previous reports have described a straight-forward treatment for determining concentration profiles from a pore relative to a collecting electrode at some distance. With limited knowledge of the geometry of the patch at the tip of the electrode, this model serves as an adequate test of the concentration-response profiles generated here. To assess the relationship between P_{open} and the Ca^{2+} ionic flux from the pore, we employed the previously derived geometric model to describe the concentration profile from a disk-shaped source (i.e., the pore).[43, 44] In the disk-shaped source model, the local ionic concentration $C(r)$ at a radical distance r from the source can be determined from eqn (1):

$$C(r) = \frac{2C_s}{\pi} \tan^{-1} \frac{\sqrt{2}a}{\sqrt{(r^2 + d^2 - a^2) + \sqrt{(r^2 + d^2 - a^2)^2 + 4d^2a^2}}} \quad (1)$$

Here C_s represents the ion concentration at the pore surface, a is the pore radius and d is the vertical distance between probe and pore surface. To compare the P_{open} curve with the Ca^{2+} concentration profile, normalized concentration [Ca^{2+}] was plotted versus vertical distance

in Figure 8b and lateral distance in Figure 9b (black curves). By comparing the profiles in Figure 8b and 9b, consistency between P_{open} and normalized [Ca^{2+}] is observed in both x and z dimensions. We are presently conducting optical microscopy and electrochemical experiments to ascertain the dimensionality of the patch at the tip, which will allow more detailed simulations to be used to predict the collection efficiency. These experiments further demonstrate the feasibility of MP-ICP for local concentration measurement of ions and molecules at submicron scales with the aid of precise positioning provided by SICM.

CONCLUSIONS

In this report, we characterized the analytical performances of the MP-ICPs to obtain a more comprehensive understanding of the system for future developments. First, MP-ICPs containing either TRPV1 channels or BK channels were constructed, which supported the generic nature of the MP-ICP platforms. We then demonstrated measurement of channel activities of both TRPV1 channels and BK channels in MP-ICP probes at the single-channel level. Results revealed that the charge of the ligand molecules plays a key role in determination of the impact of SICM barrel potential on the channel responses within the ICP barrel. For ion channels gated by uncharged ligands, such as TRPV1, channel activities were immune to the potential changes at the SICM barrel. For ion channels gated by charged ligands, such as BK, enhanced channel activities were observed when the polarity of the SICM barrel potential was opposite to the charge of the ligand molecules, and vice versa. These effects may be used to selectively enrich or deplete ions at the probe tip. Enhancement may be useful for low concentration analyte and depletion may be useful for ligand-gated ion channels with high affinity where a constant on state can be avoided. Further, the choice to intermittently disengage the SICM barrel potential may be selected. Finally, the capability of the MP-ICPs in the detection of site-specific molecular/ionic fluxes was demonstrated. In the proof-of-principle experiment, a single TRPV1 or BK channel was used as a sensor to detect molecular flux of capsaicin or ionic flux of Ca^{2+} through a pore, and the channel activities were proven to be sensitive to variations in both the vertical and lateral distances between the probe and the pore, and the P_{open} profiles correlate with the diffusional concentration profiles.

In comparison to previous reports such as those performed in the “sniffer-patch” configurations or *via* carbon electrodes, experiments performed here have two important advances. First, the probe here is manipulated with high spatial precision in x, y and z dimensions with a piezoelectric positioner, as opposed to the commonly-used manual probe control *via* a micromanipulator. Second, the use of ion channels as molecular specific sensors bypasses the limitation encountered in electrochemical detection approaches, and the analyte molecules no longer need to be electroactive to be detected, which holds promise in significantly diversify the variety of detectable molecules. At present, a detailed finite element simulation is being developed to better predict the MP-ICP response based on dimension, analyte and pipette charge, and applied potential.

The combination of the accurate probe position control with nanometer-precision afforded by SICM and the superior chemical specificity offered by the ion channels enables the study of specific ion transport with high spatial resolution at surfaces, providing exciting

opportunities to map specific molecular fluxes at cellular membranes and elucidate underlying mechanisms of cellular communication processes.

Supplementary Material

Refer to Web version on PubMed Central for supplementary material.

Acknowledgments

Indiana University and the National Science Foundation (1507341) and the National Institutes of Health (5R21EB022297-02) are acknowledged for funding. Electronic Instrument Services and Mechanical Instrument Services at Indiana University are gratefully acknowledged for assistance with instrumentation.

References

1. Wightman R, Jankowski J, Kennedy R, Kawagoe K, Schroeder T, Leszczyszyn D, Near J, Diliberto E, Viveros O. Proceedings of the National Academy of Sciences. 1991; 88(23):10754–10758.
2. Leszczyszyn DJ, Jankowski JA, Viveros OH, Diliberto EJ, Near JA, Wightman RM. Journal of Biological Chemistry. 1990; 65(25):14736–14737.
3. Adams KL, Puchades M, Ewing AG. Annu Rev Anal Chem. 2008; 1:329–355.
4. Aspinwall CA, Huang L, Lakey JR, Kennedy RT. Analytical chemistry. 1999; 71(24):5551–5556. [PubMed: 10624159]
5. Chen G, Ewing AG. Critical Reviews™ in Neurobiology. 1997; 11(1)
6. Clark RA, Ewing AG. Molecular neurobiology. 1997; 15(1):1–16. [PubMed: 9396001]
7. Pihel K, Hsieh S, Jorgenson JW, Wightman RM. Analytical chemistry. 1995; 67(24):4514–4521. [PubMed: 8633786]
8. Wightman RM. Science. 2006; 311(5767):1570–1574. [PubMed: 16543451]
9. Hume R, Role L, Fischbach G. Nature. 1983; 305(5935):632–634. [PubMed: 6621712]
10. Young SH, Poo M-m. Nature. 1983; 305(5935):634–637. [PubMed: 6312327]
11. Allen T. Trends in neurosciences. 1997; 20(5):192–197. [PubMed: 9141193]
12. Hamill OP, Marty A, Neher E, Sakmann B, Sigworth F. Pflügers Archiv European journal of physiology. 1981; 391(2):85–100. [PubMed: 6270629]
13. Crank, J. The mathematics of diffusion. Oxford university press; 1979.
14. Jiang Y, Guo W. Science Bulletin. 2015; 60(5):491–502. DOI: 10.1007/s11434-015-0739-6
15. Zhou Y, Bright LK, Shi W, Aspinwall CA, Baker LA. Langmuir. 2014; 30(50):15351–15355. [PubMed: 25425190]
16. Macazo FC, White RJ. Journal of the American Chemical Society. 2016; 138(8):2793–2801. [PubMed: 26848947]
17. Hansma PK, Drake B, Marti O, Gould S, Prater C. Science. 1989; 243(4891):641. [PubMed: 2464851]
18. Chen CC, Zhou Y, Baker LA. Annual Review of Analytical Chemistry. 2012; 5:207–228.
19. Shi W, Zeng Y, Zhou L, Xiao Y, Cummins TR, Baker LA. Faraday Discussions. 2016; 193:81–97. [PubMed: 27711908]
20. Marty A. Nature. 1981; 291(5815):497–500. [PubMed: 6262657]
21. Caterina MJ, Schumacher MA, Tominaga M, Rosen TA, Levine JD, Julius D. Nature. 1997; 389(6653):816–824. [PubMed: 9349813]
22. Chen C, Okayama H. Molecular and Cellular Biology. 1987; 7(8):2745–2752. DOI: 10.1128/mcb.7.8.2745 [PubMed: 3670292]
23. Xiao Y, Bingham J-P, Zhu W, Moczydlowski E, Liang S, Cummins TR. Journal of Biological Chemistry. 2008; 283(40):27300–27313. [PubMed: 18628201]
24. Basbaum AI, Bautista DM, Scherrer G, Julius D. Cell. 2009; 139(2):267–284. [PubMed: 19837031]

25. Dubin AE, Patapoutian A. The Journal of clinical investigation. 2010; 120(11):3760–3772. [PubMed: 21041958]
26. Vriens J, Appendino G, Nilius B. Molecular pharmacology. 2009; 75(6):1262–1279. [PubMed: 19297520]
27. Ramsey IS, Delling M, Clapham DE. Annu Rev Physiol. 2006; 68:619–647. [PubMed: 16460286]
28. Julius D. Annual review of cell and developmental biology. 2013; 29:355–384.
29. Hazan A, Kumar R, Matzner H, Priel A. Scientific reports. 2015; 5:12278. [PubMed: 26194846]
30. Szallasi A, Blumberg PM. Pharmacological reviews. 1999; 51(2):159–212. [PubMed: 10353985]
31. Jung J, Hwang SW, Kwak J, Lee SY, Kang CJ, Kim WB, Kim D, Oh U. Journal of Neuroscience. 1999; 19(2):529–538. [PubMed: 9880573]
32. Premkumar LS, Agarwal S, Steffen D. The Journal of physiology. 2002; 545(1):107–117. [PubMed: 12433953]
33. Caterina MJ, Julius D. Annual review of neuroscience. 2001; 24(1):487–517.
34. Liao M, Cao E, Julius D, Cheng Y. Nature. 2013; 504(7478):107–112. [PubMed: 24305160]
35. Adelman JP, Shen KZ, Kavanaugh MP, Warren RA, Wu YN, Lagrutta A, Bond CT, North RA. Neuron. 1992; 9(2):209–216. [PubMed: 1497890]
36. Atkinson NS, Robertson GA, Ganetzky B. Science. 1991; 253(5019):551–556. [PubMed: 1857984]
37. Latorre R, Miller C. Journal of Membrane Biology. 1983; 71(1):11–30. [PubMed: 6300405]
38. Cao E, Liao M, Cheng Y, Julius D. Nature. 2013; 504(7478):113–118. [PubMed: 24305161]
39. Salkoff L, Butler A, Ferreira G, Santi C, Wei A. Nature Reviews Neuroscience. 2006; 7(12):921–931. [PubMed: 17115074]
40. Carvacho I, Gonzalez W, Torres YP, Brauchi S, Alvarez O, Gonzalez-Nilo FD, Latorre R. The Journal of general physiology. 2008; 131(2):147–161. [PubMed: 18227273]
41. van Welie I, du Lac S. Journal of neurophysiology. 2011; 105(4):1651–1659. [PubMed: 21307321]
42. Pallotta BS, Magleby KL, Barrett JN. Nature. 1981; 293(471):471. [PubMed: 6273730]
43. Scott ER, White HS, Phipps JB. Analytical chemistry. 1993; 65(11):1537–1545. [PubMed: 8328671]
44. Chen C-C, Baker LA. Analyst. 2011; 136(1):90–97. DOI: 10.1039/C0AN00604A [PubMed: 21103593]

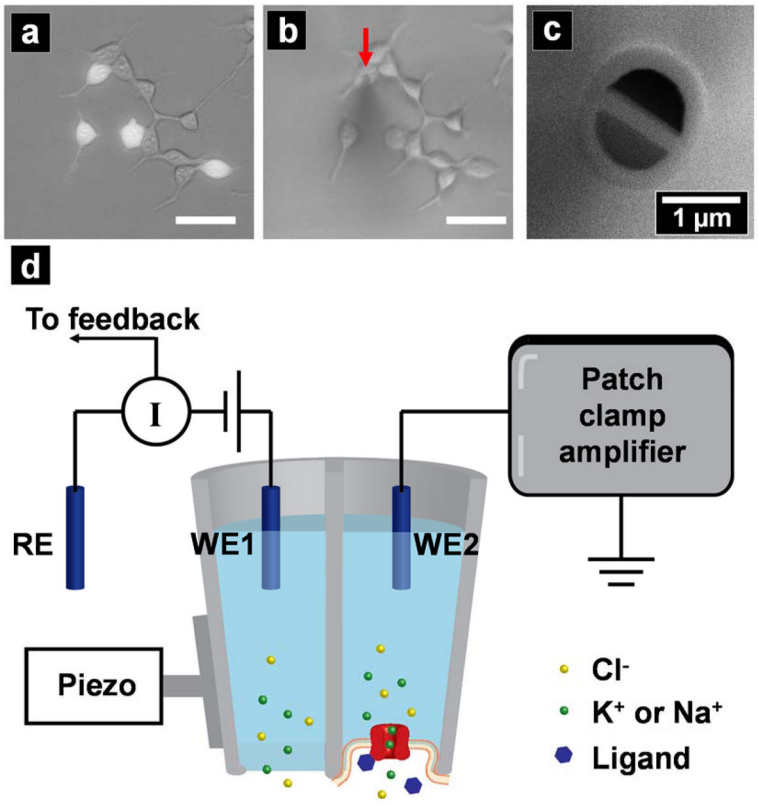

Figure 1.

(a) Overlaid fluorescence image and bright-field image of HEK 293 cells co-transfected with TRPV1 and GFP; (b) bright-field image of the area seen in (a) after formation of tight seal between the probe and the cell, with the position of the probe indicated by a red arrow for better visualization. Scale bar = 50 μm; (c) scanning electron micrograph of a theta pipette showing an end-on view; (d) instrumental set-up for the dual-barrel ICP-SICM measurements.

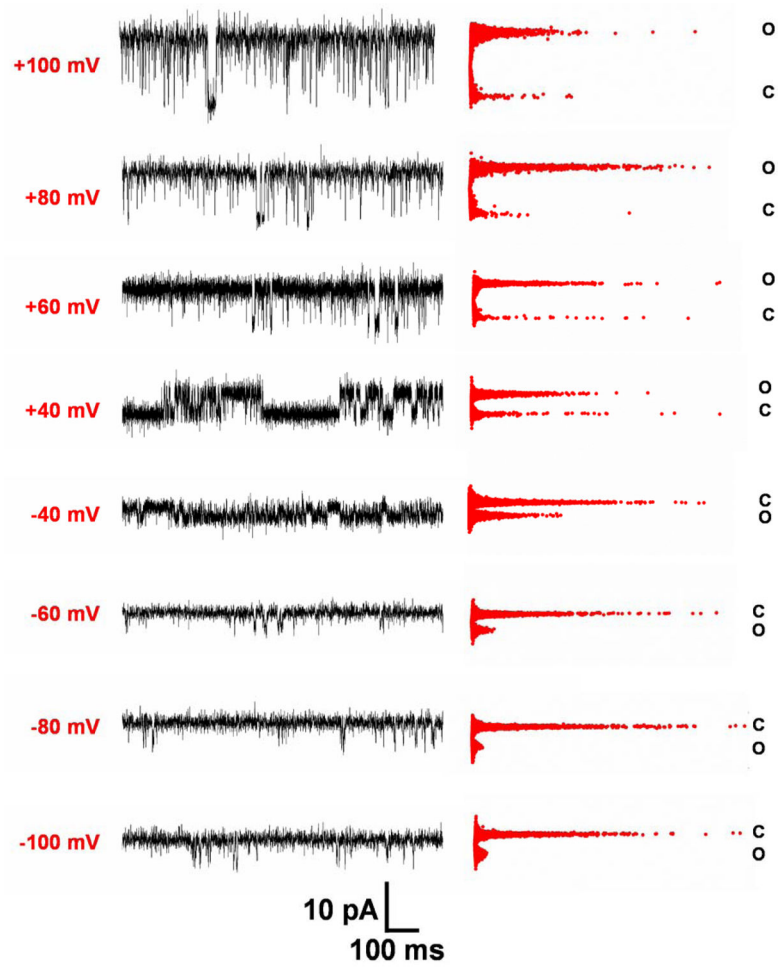

Figure 2.

Current-time (I–T) traces (left) and corresponding statistical graphs (right) of amplitude (I_{open}) vs. dwell time (t_{open}) recorded *via* a TRPV1 channel at different membrane potentials. C: closed state; O: open state.

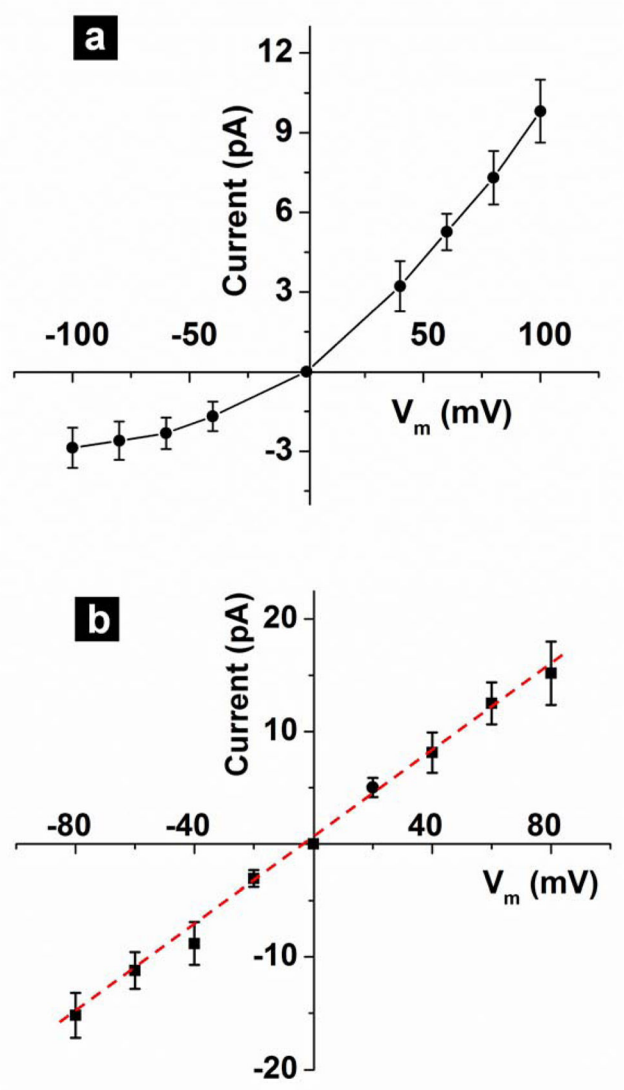

Figure 3.

(a) Current-voltage (I–V) relationship TRPV1 channels derived from I–T measurements from an inside-out membrane patch; (b) I–V relationship of BK channels derived from I–T measurements from an inside-out membrane patch.

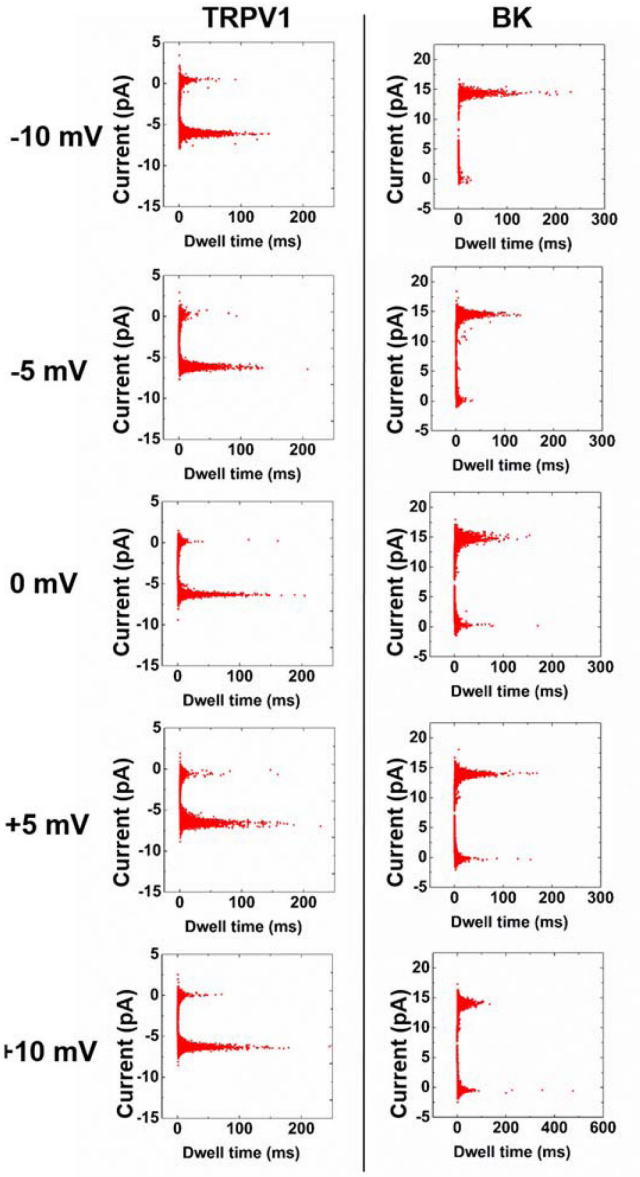

Figure 4.

Statistical graphs of I_{open}-t_{open} for TRPV1 (left) and BK (right), when the potential applied to the SICM barrel was held at −10 mV, −5 mV, 0 mV, +5 mV and +10 mV. V_m = +60 mV for ICP barrel.

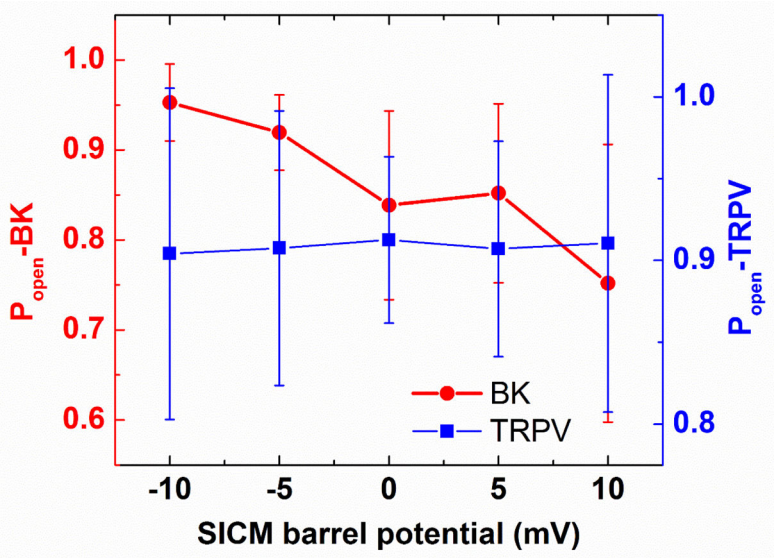

Figure 5.

Plots of P_{open} vs. SICM barrel potential for TRPV1 (blue) and BK (red). V_m = +60 mV for ICP barrel.

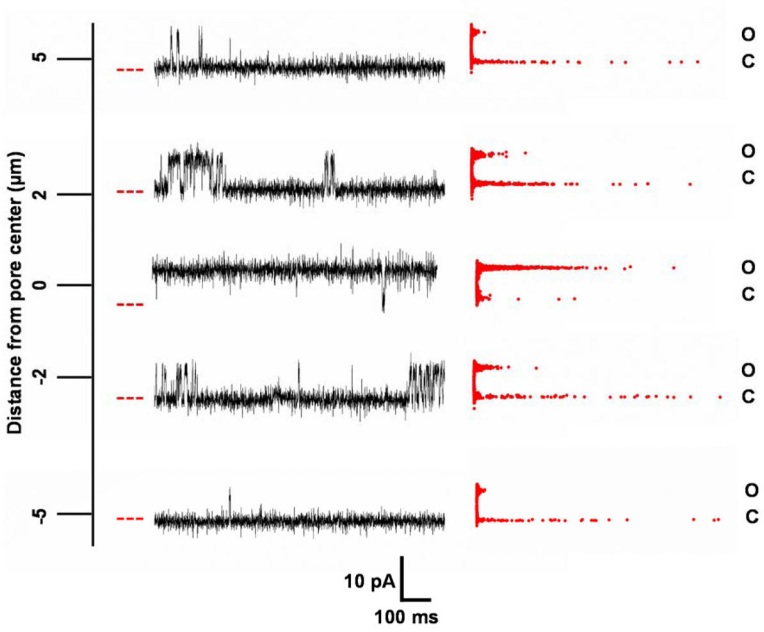

Figure 6.

Representative I–T traces and corresponding statistical graphs of I_{open}-t_{open} recorded *via* a single TRPV1 channel at the ICP barrel, at varying lateral displacements between the probe and the nanopore, i.e., the capsaicin source.

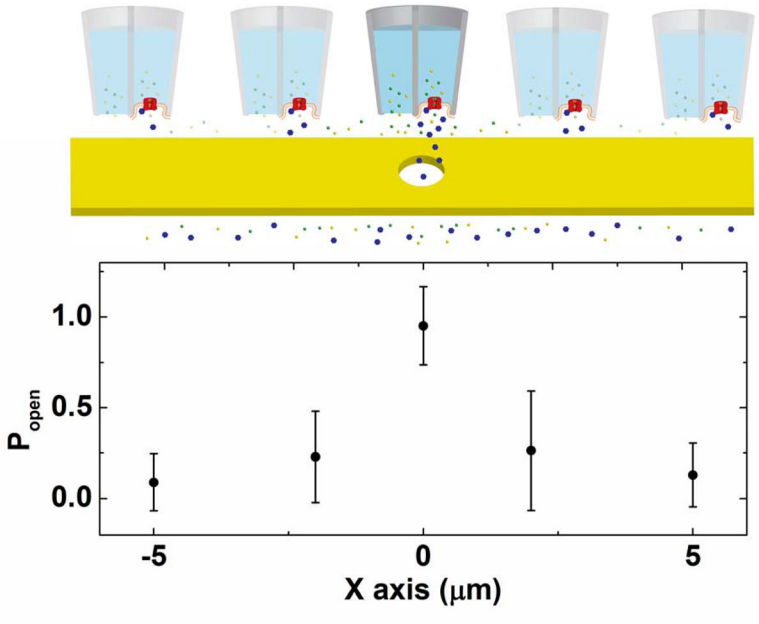

Figure 7.

(Top) Cartoon illustration to show the relative position of the MP-ICP probe to the nanopore during experiments; (bottom) plot of P_{open} vs. lateral displacement between the probe and the nanopore obtained *via* a single TRPV1 channel held at V_m = +60 mV.

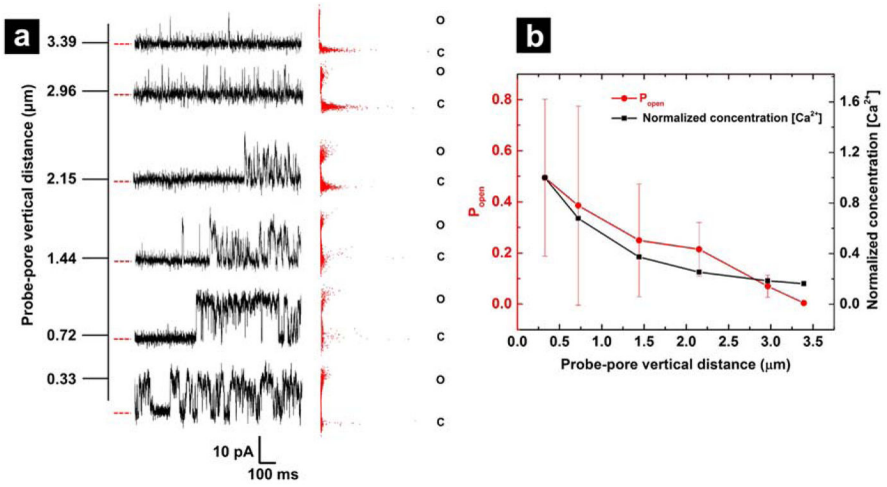

Figure 8.

(a) Representative I–T traces and corresponding statistical graphs of I_{open}-t_{open} recorded *via* a single BK channel at the ICP barrel, at varying vertical distances between the probe and the pore surface, i.e., the Ca^{2+} source. (b) P_{open} profile (red) and normalized [Ca^{2+}] profile (black) calculated from the disk-shaped source model.

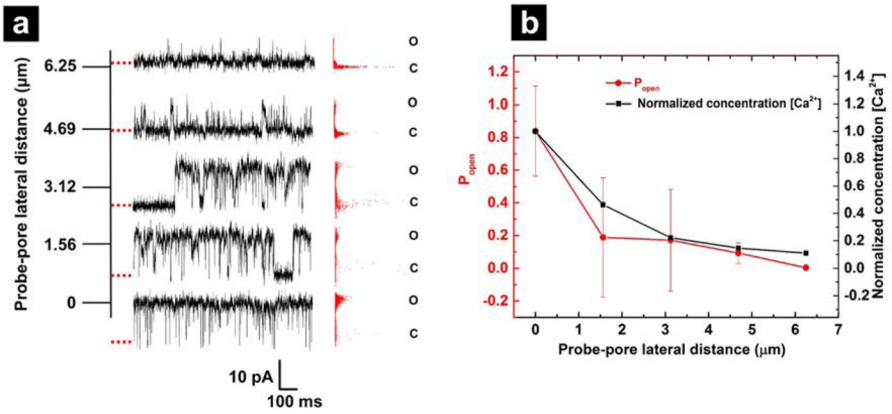

Figure 9.

(a) Representative I–T traces and corresponding statistical graphs of I_{open}-t_{open} recorded *via* a single BK channel at the ICP barrel, at varying lateral distances between the probe and the pore center. (b) P_{open} profile (red) and normalized $[Ca^{2+}]$ profile (black) calculated from the disk-shaped source model.